

# Subpulse Drifting, Nulling and Mode changing in PSR J2006–0807 with Core emission

Rahul Basu<sup>1,2</sup>, Ashis Paul<sup>3</sup>, Dipanjan Mitra<sup>3,2</sup>

<sup>1</sup> *Inter-University Centre for Astronomy and Astrophysics, Pune, 411007, India; rahulbasu.astro@gmail.com*

<sup>2</sup> *Janusz Gil Institute of Astronomy, University of Zielona Góra, ul. Szafrana 2, 65-516 Zielona Góra, Poland*

<sup>3</sup> *National Centre for Radio Astrophysics, Tata Institute of Fundamental Research, Pune 411007, India*

1 May 2019

## ABSTRACT

We report a detailed analysis of the emission behaviour of the five component, core-double cone, pulsar J2006–0807 (B2003–08). The single pulses revealed the presence of the three major phenomena of subpulse drifting, nulling and mode changing. The pulsar switched between four different emission modes, two of which showed systematic drifting with prominent drift bands, and were classified as modes A and B respectively. The drifting was seen primarily in the conal components and exhibited the rare phenomenon of bi-drifting, where the drift direction in the second component was opposite to the fourth component. This made PSR J2006–0807 the only known example where systematic drift bands were seen around a central core emission. The emission showed a gradual decrease in intensity during mode A which stabilised to a relatively constant level in the subsequent mode B. The presence of a low frequency, weak and wide structure in the fluctuation spectra was also seen primarily in the core component during modes A and B. The core component vanished during mode C and was most prominent during the fourth mode D. Both these modes were frequently interspersed with null pulses. No detectable drifting was seen during modes C and D, but the pulsar showed short duration periodic nulling in the core as well as the conal components. In addition to the four emission modes the pulsar also nulled for long durations lasting up to hundred rotation periods.

**Key words:** pulsars: individual: J2006–0807 (B2003–08).

## 1 INTRODUCTION

The single pulse sequences in the radio emission from certain pulsars are characterised by the three prominent phenomena of nulling, mode changing and subpulse drifting. The nulling and mode changing are seen as sudden changes in the emission state within a few rotation periods. The emission changes to a different profile shape in case of mode changing, while during nulling the radio emission completely ceases for certain durations. The subpulse drifting on the other hand is seen as a periodic pattern within the pulse window where the subpulses show gradual shift resembling drift bands. The average profile is expected to be representative of the radio emission region of the magnetosphere, which is approximated as an emission beam. The emission beam comprises of a central core component, surrounded by nested rings of conal emission (Rankin 1993; Mitra & Deshpande 1999; Mitra & Rankin 2002). Recent studies have shown the core and conal components to originate from similar emission heights (Maciesiak *et al.* 2012; Skrzypczak *et al.* 2018). The shape of the average profile depends on the line of sight (LOS) traverse of the emission beam. The profile shape can be categorised as conal single ( $S_d$ ), conal Double (D), conal Triple ( $cT$ ), conal Quadruple ( $cQ$ ), core-cone

Triple (T) and core-double cone Multiple (M) with five components. This corresponds to the different LOS traverses progressively from the edge of the emission beam towards the center. There are also the core single ( $S_t$ ) profiles, with central LOS traverse, where the conal emission are too weak to be detected at frequencies below 1 GHz (Mitra & Rankin 2017). A number of pulsars have now been reported where the pulsar transitions between different emission modes with some of them exhibiting drifting. The examples of such pulsars are B0031–07 (Vivekanand & Joshi 1997; Smits *et al.* 2005; McSweeney *et al.* 2017), B1918+19 (Hankins & Wolszczan 1987; Rankin *et al.* 2013), B1944+17 (Kloumann & Rankin 2010), J1822–2256 (Basu & Mitra 2018b) and B2319+60 (Wright & Fowler 1981). These pulsars show a wide variety in their profile shapes but they all have conal profiles.

There are very few studies which report similar behaviour in core-cone pulsars, particularly with M type profiles, with B1237+25 one of the few well studied examples of a five component pulsar showing presence of subpulse drifting as well as mode changing (Backer 1970; Srostlik & Rankin 2005; Smith *et al.* 2013; Maan & Deshpande 2014). The presence of subpulse drifting and two emission modes has also been reported for the pulsar

B1737+13, which has five components with a central core emission (Force & Rankin 2010). However, in none of these cases the pulsar shows multiple emission modes with systematic drift bands and nulling. This has led to a number of generalized assumptions about the radio emission in the presence of core component. For example, it has been suggested that the drifting is primarily phase stationary for the central line of sight traverse of the emission beam, corresponding to T and M profiles (Rankin 1986; Gil & Sendyk 2000). The systematic drift bands are only possible in conal profiles with peripheral line of sight traverses of the emission beam. Additionally, the appearance of periodic nulling in certain pulsars has been seen in primarily conal profiles. An association between periodic nulls and drifting has been proposed, with the periodic nulls also termed as pseudo-nulls. They are postulated to originate due to the line of sight traverses between empty regions of a rotating sub-beam system (Herfindal & Rankin 2007, 2009). Detailed observations of pulsars with core emission in recent works suggest that revisions of our prevalent understanding of the emission processes are necessary. Basu *et al.* (2019) has studied the phase behaviour of drifting in pulsars with core components and found significant phase variations in the corresponding conal components. It has also been shown by Basu *et al.* (2016, 2017) that the drifting periodicity is inversely proportional to the spin-down energy loss ( $\dot{E}$ ), while the periodicity associated with nulling show no such dependence. This suggests different physical mechanisms responsible for the two phenomenon. However, the biggest challenge has been to find a pulsar with core emission which show clear evidence of drift bands in addition to multiple emission modes and nulling in the same system. This would enable us to directly study the emission processes for central line of sight traverse of the emission beam.

The pulsar J2006–0807 (B2003–08) has a prominent core component with clearly resolved inner and outer cones, and belongs to profile class M. The pulsar was observed as part of the Meter-wavelength Single-pulse Polarimetric Emission Survey (MSPES, Mitra *et al.* 2016). The pulsar exhibited subpulse drifting whose average behaviour was reported in Basu *et al.* (2016). In addition, the single pulses indicated the presence of nulling as well as mode changing. The pulsar has the potential to be an exemplar of the intricate emission processes like multiple mode changing, nulling and subpulse drifting, in core profiles, which have previously been associated with conal only pulsars. To study these phenomena in more detail we have carried out sensitive observations of a large number of single pulses from this pulsar. We have carefully analysed the single pulse behaviour to characterise the different phenomena seen in this system. In section 2 we report the observational details; section 3 details the nulling and mode changing analysis; section 4 presents the polarization behaviour and our estimates of LOS geometry; in section 5 we present the drifting behaviour; section 6 presents an in depth discussion of the implications of these results on the prevalent understanding of the radio emission process and finally we summarize our results in section 7.

## 2 OBSERVING DETAILS

As mentioned above the pulsar J2006–0807 has been observed as part of MSPES, which recorded polarized single pulses using the Giant Meterwave Radio Telescope (GMRT), located near Pune in India (Swarup *et al.* 1991). The observing details of MSPES is reported in Mitra *et al.* (2016). The survey observed 123 pulsars at two frequencies, 333 and 618 MHz, over a 16 MHz bandwidth, for roughly 2100 pulses. The pulsar J2006–0807 has a

period of around 0.58 seconds and a low dispersion measure of  $32.39 \text{ pc cm}^{-3}$ . The MSPES observations were sensitive to detect single pulses at 333 MHz for this pulsar, while only the average profile was measured at 610 MHz. We have carried out further observations at 339 MHz using the GMRT to characterize the emission properties of PSR J2006–0807 in more detail. These observations were conducted on 18 November 2017, and recorded around 4800 single pulses. In order to record more sensitive single pulses we observed using a 33 MHz bandwidth. However, this implied that the full polarization signals could not be recorded without significant loss due to the higher data rates, and hence we only observed in the total intensity mode for the newer observations. A number of detailed steps were followed to convert the recorded signals to a frequency averaged single pulse sequence. This included removing the radio frequency interference from the time sequence as well as frequency channels, averaging across the frequency band after correcting for the dispersion spread, using the known dispersion measure, and finally re-sampling the band averaged data to two dimensional pulse stack with the x-axis corresponding to the longitude bins and the y-axis the pulse numbers. The details of observational techniques as well as the initial analysis is presented in our earlier works (see e.g. Basu *et al.* 2016, 2017; Basu & Mitra 2018a). The final pulse stack was used for the different analysis described in the subsequent sections. In addition, we also used the polarization information from the 333 MHz MSPES observations to estimate the pulsar geometry and emission properties as reported in section 4.

## 3 MODE CHANGING AND NULLING

### 3.1 The Emission Modes

A wide variety of single pulse behaviour was seen in this pulsar, with frequent transitions from one emission mode to another. We have carried out a rigorous evaluation of the mode changing phenomenon by careful inspection of the single pulse sequence. In most of the cases we were able to identify the emission modes by visually inspecting them. But there were instances where the modal boundaries were overlapping, or the pulsar nulling made it difficult to make such distinctions. Short duration sequences ( $< 10$  periods) were not classified as distinct modes due to the apparent ambiguity in such identifications. We have identified four clear emission modes as shown in figure 1. The most noticeable emission modes were characterised by the presence of subpulse drifting with prominent drift bands seen in the inner conal pairs, comprising of the second and fourth component, as seen in the left panel of the figure. The drifting behaviour showed a gradual transition, with the periodicity changing to almost half of the initial value. However, the boundary of this transition was not sharp and extended over several pulse periods. We have classified the drifting state into two modes, where the initial longer periodicity drifting at the start of the emission was termed as mode A and the later shorter periodic state was identified as mode B. The outer cones, comprising of the first and fifth component, also showed similar periodicity during the two modes, but the fluctuations were more phase stationary without any clear drift bands. A more detailed analysis of the drifting behaviour of modes A and B is presented in section 5 where we have also listed the pulse ranges when the modes are seen in the single pulse sequence. In addition to the conal variations the central core emission also underwent significant change during the two modes. As shown in the average modal profiles in figure 2 (top left panel), the core emission was much stronger during mode A and

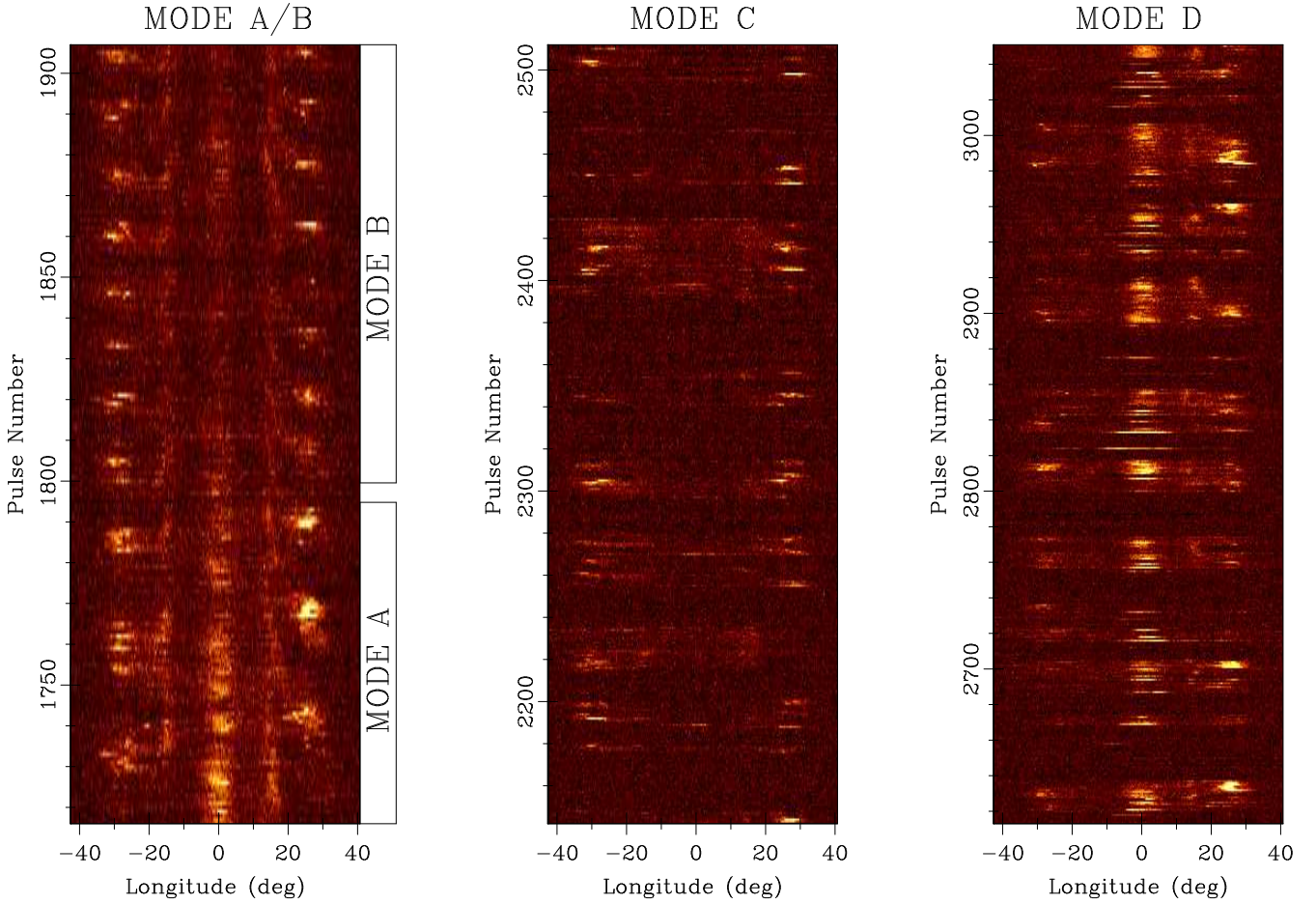


**Figure 1.** The figure represents the different emission modes seen in PSR J2006–0807. The two modes A and B show the presence of systematic subpulse drifting with different periodicities and mode B is usually seen following mode A. The left window represents a section of the pulse stack ranging from pulse number 1716 to 1907, and shows the two modes A and B. Mode A gradually transitions into mode B without a clear boundary. Though no clear nulling is seen during this sequence, it is seen in the pulses immediately preceding and following this region. The middle panel shows the sequence of pulses ranging from pulse number 2142 to 2512 and represents mode C. The core emission is almost non-existent in this mode which is frequently interspersed with null pulses. An example of mode D is shown in the right panel which represents the stack from pulse number 2613 to 3051. The emission mode is characterised by the presence of the strong core component. Similar to previous case, frequent nulling is also seen during mode D.

became comparable to the conal emissions in mode B (see the top right panel of the figure 2). The conal emissions were also brighter in mode A compared to mode B. During the 4800 periods of observations we found three sequences, similar to left panel in figure 1, where the two modes coexisted. These sequences lasted between 200 and 300 pulses, with mode A typically spanning the first 100 pulses. In figure 3 we show variation in the intensities of the core and inner conal component at the single pulse level, as the pulsar transitioned from mode A to mode B. Both the core and the conal components were brighter at the start of mode A and the intensity gradually decreased during the mode. During mode B a roughly constant intensity with time was seen in the different components. In addition there were another eight sequences where the mode A was seen lasting between 40-100 periods, but instead of changing over to mode B the pulsar started nulling or moved to a different emission mode immediately afterwards. Additionally, another three sequences were found, separated by long nulls between pulse number 4050 and 4365, where only mode B was seen for durations between 40 and 80 pulses, without the preceding mode A. To summarize, during this observation the pulsar lasted for around 15% of time in mode A with an average mode duration of 65 periods. The

corresponding abundance of mode B was around 13% and the average modal length was roughly 103 periods. The modal behaviour in the MSPES, 333 MHz observations of roughly 2100 periods, were very different. It was difficult to ascertain the emission modes due to the lower sensitivity of the detections. However, we found one long sequence of emission in mode B lasting around 510 periods, preceded by a roughly 50 period long mode A. This was found near the beginning of the observations. No other clear drifting state was found for the remainder of these observations. This also implied that mode B had the possibility of lasting for much longer durations than seen in the later observation.

In addition to the distinct drifting modes the pulsar also showed the presence of two emission states which did not show any drift bands. However, there were still periodic modulations associated with these states which are explored in the next subsection 3.2. The third mode C was characterised by the absence of a clear core emission which was very weak. In figure 1, middle panel, a roughly 370 period duration of the pulse sequence in mode C is shown. The emission was frequently disrupted by the presence of nulls. The emission was only seen for short durations with the minimum being a few periods and the maximum duration of roughly thirty periods.

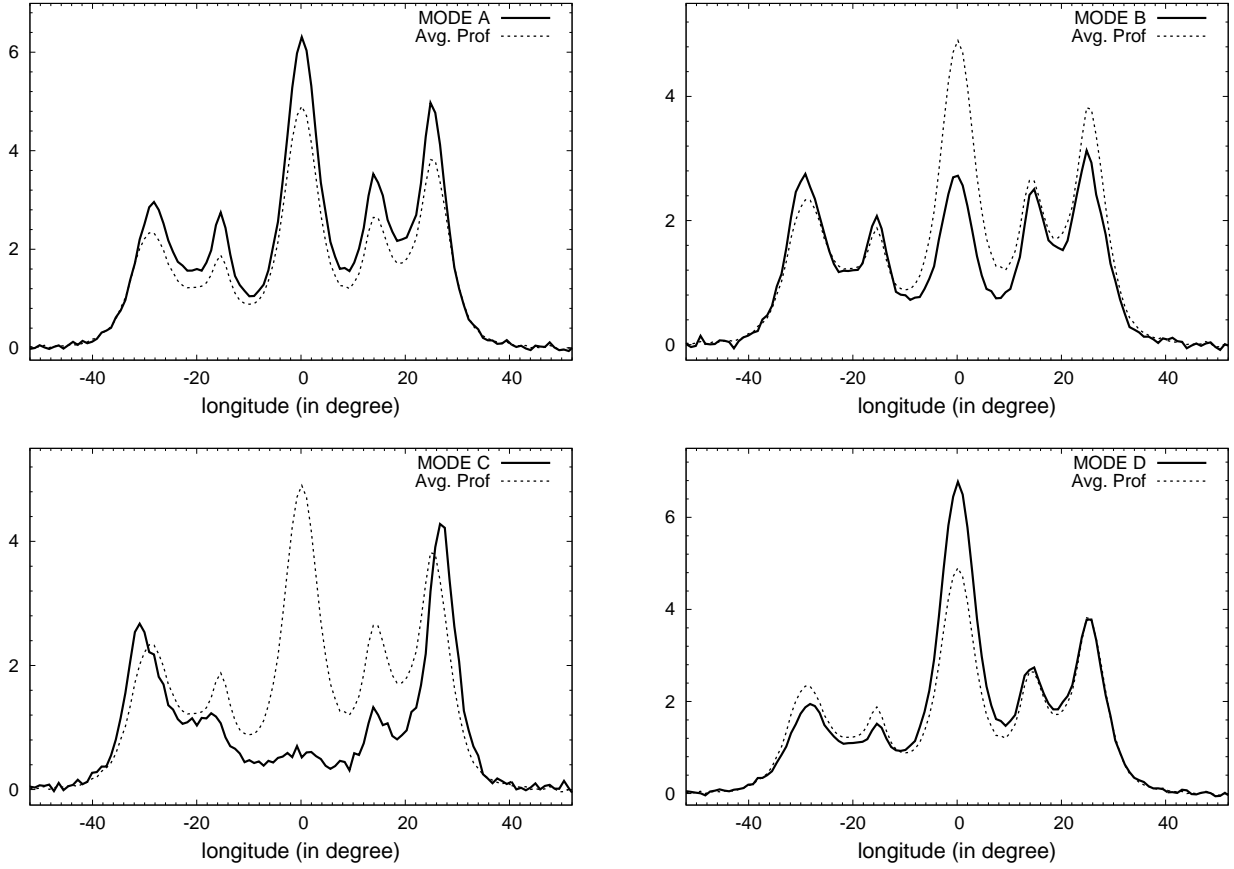


**Figure 2.** The figure shows the profile of each of the four modes present in the pulsar J2006–0807 along with the average profile for comparison. The top left panel shows the profile corresponding to mode A, which has a strong core emission and the conal components are also prominent. The top right panel corresponds to mode B which has a much weaker core component, but the core is still comparable to the cones. The bottom left panel shows the profile of mode C, where the core is almost non-existent and the inner conal pairs are also much weaker. Finally, the mode D profile is shown on the bottom right panel and is characterised by the strongest core component. The extent of the profiles does not change in the different modes, with the outermost extremes coincident with the average profile in each case.

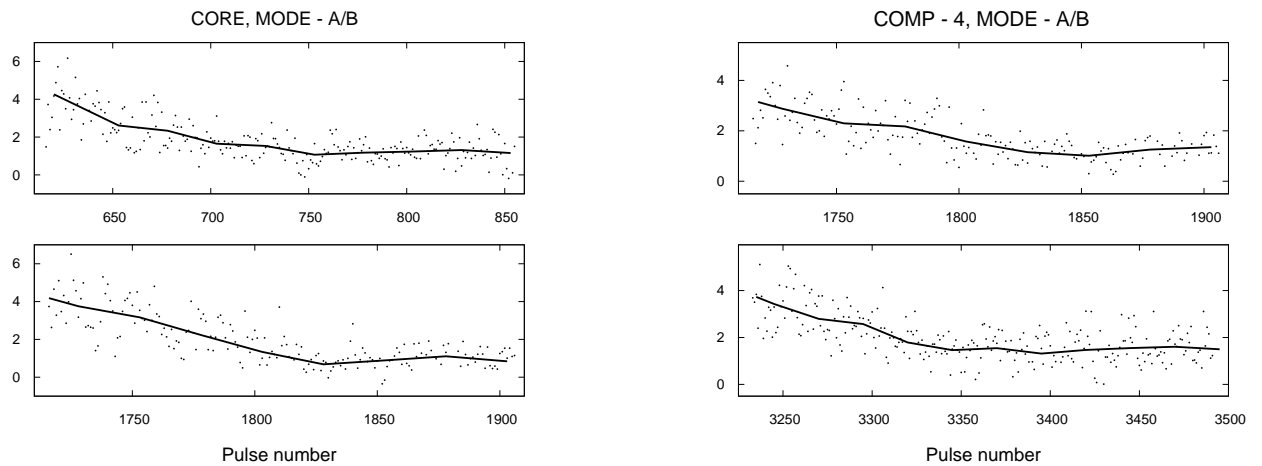


**Figure 3.** The figure shows variation of the component intensities during transitions from modes A to mode B. The left panel shows the variation of the core energy during two sequences, between pulse 616 and 855 (top window), and pulse 1716 and 1907 (bottom window), where the pulsar transitions from mode A and B. The average energy in the core window for each pulse is shown as a dot while the solid line represents the trend of the energy evolution with time. The right panel shows an equivalent plots for the inner conal component ( $4^{th}$  component), corresponding to two sequences, between pulse 1716 and 1907 (top window), and pulse 3233 and 3494 (bottom window). The intensities in each component window gradually decreases from the start of mode A and stabilizes to a roughly constant level in mode B.

**Table 1.** Emission Mode durations in PSR J2006–0807

Pulse Range (P)	MODE	Duration (P)
12 - 33	D	22
67 - 83	C	17
100 - 160	A	61
211 - 232	C	22
273 - 472	D	200
505 - 528	C	24
569 - 592	A	24
603 - 613	D	11
616 - 856	A-B	241
910 - 953	A	44
954 - 1376	D	423
1425 - 1455	A	31
1491 - 1715	D	225
1716 - 1907	A-B	192
1981 - 2022	D	42
2031 - 2122	A	92
2142 - 2512	C	371
2618 - 3229	D	612
3233 - 3494	A-B	262
3525 - 3592	D	68
3641 - 3784	A-B	144
3688 - 3700	D	13
3795 - 3813	C	19
3851 - 3885	D	35
3942 - 3968	A	27
3972 - 3996	D	25
4045 - 4057	D	13
4058 - 4130	B	73
4137 - 4154	C	18
4188 - 4240	B	53
4379 - 4439	C	61
4519 - 4528	D	10
4539 - 4554	C	16
4585 - 4600	D	16
4614 - 4623	C	10
4702 - 4798	A	97

The average duration of this mode was around 16 periods and the modal abundance was around 7%. In figure 2, bottom left panel, the average profile of mode C is shown. In addition to the lack of a proper core emission, the profile also reveals that the inner conal pairs were also significantly weaker. Only the outer cones were comparable in intensity with the other modes. Finally, the fourth distinct mode present in the pulsar, mode D, was characterised by the presence of strong core emission. In figure 1, right panel, a section of the sequence of around 440 pulses belonging to this mode is shown, which clearly highlights the strong core component. Similar to mode C, and unlike modes A and B, this mode also showed interspersed null pulses. The mode durations were also similar to mode C, with minimum duration of a few periods and maximum of around 35 consecutive pulses. The average mode duration was 15 periods and the pulsar existed for roughly 22% of time in mode D. The average profile of this mode, as shown in 2, bottom right panel, also reveals that in addition to a strong component, the strongest of the three modes, the conal emission was also slightly asymmetric. The trailing pair of conal components, corresponding to the fourth and fifth components, were more prominent than the leading ones, similar to mode A. Table 1 lists the pulse sequences during

**Table 2.** Characterising the emission modes in PSR J2006–0807

MODE	%	Avg. Duration (P)	$W_{50}$ (°)	$W_{5\sigma}$ (°)
A	15	65	$60.9 \pm 1.3$	$73.9 \pm 1.3$
B	13	103	$62.1 \pm 1.3$	$72.4 \pm 1.3$
C	7	16	$64.4 \pm 1.3$	$73.2 \pm 1.3$
D	22	15	$62.0 \pm 1.3$	$76.8 \pm 1.3$

each emission mode along with the duration of the modes<sup>1</sup>. In case there were nulls between emission states in the same mode, they have been included in the modal duration estimates. However, the nulls on the boundary of two emission modes were not included. In Table 2 we have summarized the modal behaviour of the pulsar, including the relative abundance, the average duration of each mode as well as the 50% width ( $W_{50}$ ) and  $5\sigma$  width ( $W_{5\sigma}$ ) of the mode profiles. The profile widths are largely similar for the different modes indicating similar emission altitudes.

### 3.2 Nulling

The nulling in PSR J2006–0807 was reported for the first time in Basu *et al.* (2017) using the MSPES data. The nulling fractions were reported to be  $15.6 \pm 1.0\%$  at 333 MHz and  $24.2 \pm 1.5\%$  at 618 MHz, respectively, which indicates a wide variation. However, due to the lower sensitivity of these observations no further analysis could be conducted. We have used the more sensitive 18 November, 2017, observations to carry out a detailed nulling analysis of this pulsar employing the methods detailed in Basu *et al.* (2017); Basu & Mitra (2018b). The energy distributions of the single pulses and a suitably selected off-pulse window were estimated, as shown in figure 4 (top window). The on-pulse energies showed a double peaked structure with the null pulses showing a peak coincident with the off-pulse distribution. We estimated suitable Gaussian approximations for the off-pulse as well as the null energy distributions which were used to estimate the nulling fraction. The individual null and burst pulses were initially identified from the statistical boundary of the off-pulse distribution. Subsequently, all statistically identified nulls were visually inspected to search for low level emission and any such cases were reclassified as burst pulses. The nulling fraction was  $36.2 \pm 2.8\%$  for the 339 MHz observations. This value is higher than the previous measurements. As reported in the previous subsection 3.1, the MSPES observations at 333 MHz contained a long duration of mode B, with lower incidence of nulling compared to mode C and D. This likely resulted in underestimation of the nulling fraction. In case of the 618 MHz observations, the nulling fraction is higher than the 333 MHz value but lower than our latest measurements. However, the single pulses in this case were too weak to explore the modal behaviour. The combined nulling fraction of the three observations is  $28.6 \pm 3.4\%$ . In the bottom window of figure 4 we show the profiles formed after averaging the null and burst pulses separately. There is no detectable emission seen coinciding with any of the components during nulling which justifies our identification scheme for the null and burst pulses. The amount by which the radio emission is decreased during nulling is given by the factor  $\eta$ . It is estimated as  $\eta = \Sigma P(i) / 3\sigma_N$ , here  $P(i)$  is the measured intensity along the

<sup>1</sup> The processed single pulse data has been made publicly available and can be downloaded from : <ftp://ftpnkn.ncra.tifr.res.in/dmitra/J2006-0807/>

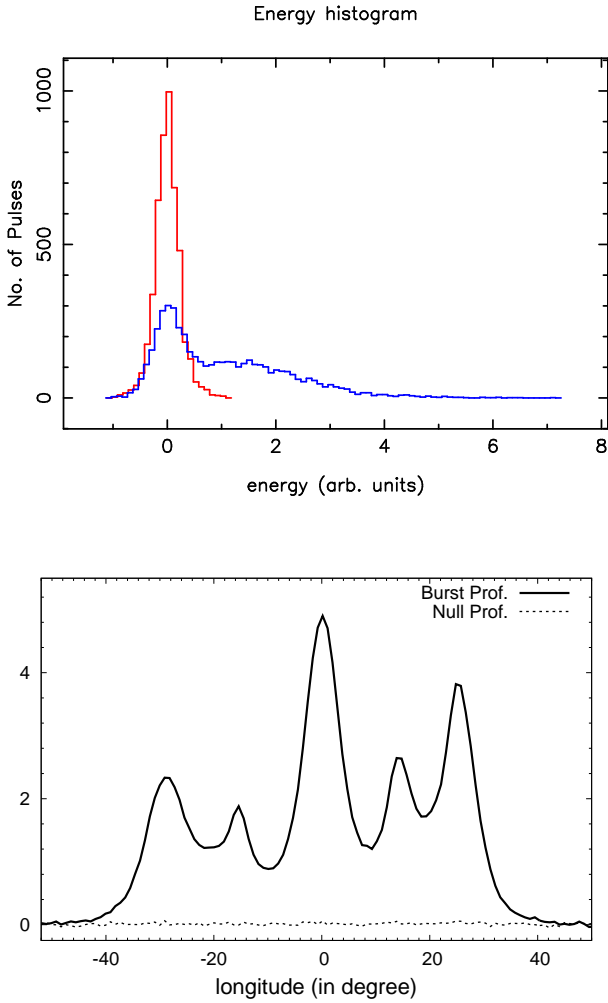


**Figure 4.** The figure shows the nulling analysis for the pulsar J2006–0807. The average energy distribution corresponding to the pulse window (blue) as well as the off-pulse noise (red) is shown on the top window. The on-pulse energies show a bimodal distribution with the null pulse distribution coincident with the off-pulse. In the bottom panel of the figure we have shown the folded profile corresponding to the null and burst pulses. The null profile is noise like which indicates that no low level emission was present during nulling.

$i^{\text{th}}$  bin of the pulse window for the burst profile and  $\sigma_N$  is the rms in the equivalent window of the null profile. The estimated value is  $\eta = 2577.5$ , which is one of the highest reported in the literature (see Vivekanand & Joshi 1997; Gajjar *et al.* 2012).

The high significance of the single pulse detection during the 18 November, 2017 observations at 339 MHz enabled us to estimate the durations of the null and burst events. There were around 260 transitions between nulling and bursting during the 4800 periods. In figure 5 the distributions of the null and burst lengths are shown. The two distributions are dominated by short duration nulls and bursts which are consistent with previously measured distributions (see Basu *et al.* 2017). In addition longer duration nulls of 50-100 periods was seen in a few cases. As discussed in the previous subsection 3.1, the longer duration bursts between 50 and 250 periods occurred during modes A and B. The other two modes C and D were frequently interrupted by short nulls. The average null

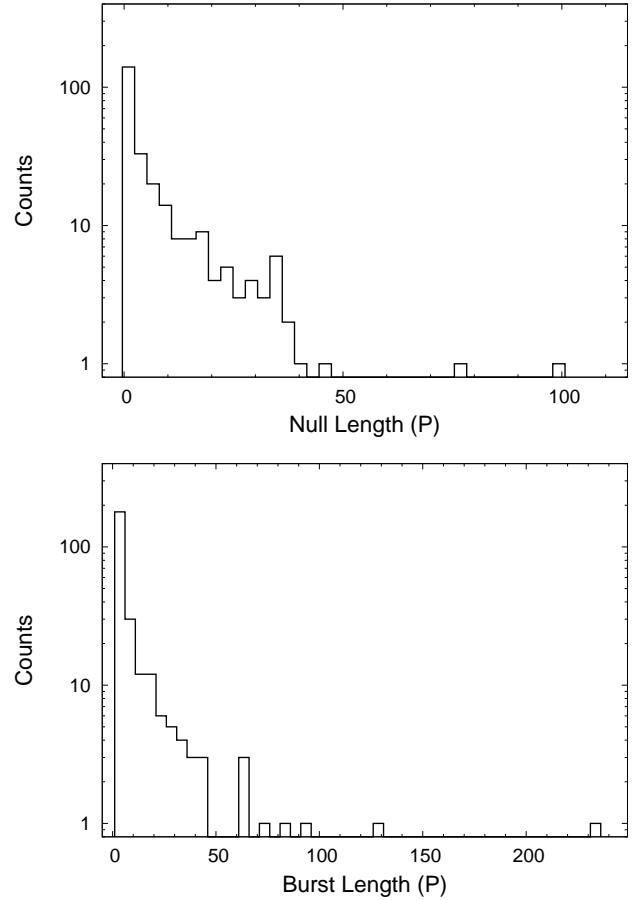


**Figure 5.** The figure shows the distributions of the null length (top panel) and burst length (bottom panel) for the duration of our observations. The distributions are dominated by short duration nulls and bursts. The null length histogram shows evidence of long intervals of nulls lasting 50-100 periods at a time. The burst length histogram also shows several long intervals ranging from 50 to 200 periods. These correspond to the modes A and B of the pulsar. The lower range below 20 periods, on the other hand, are mainly due to modes C and D.

length was 8.3 periods, while the average burst length was of 9.8 period duration.

In addition to the subpulse drifting seen in modes A and B, the pulsar also showed a low frequency feature in the average fluctuation spectra (Basu *et al.* 2016). However, due to the presence of a large number of modes with different periodic features, the low frequency feature could not be resolved in the earlier work. We have now carried out a detailed study of the individual modes to investigate the origin of this periodicity in more detail. The fluctuation spectra corresponding to mode A and B has been investigated to evaluate the drifting behaviour. In case of these two modes no low frequency feature was seen and the only periodicity was due to the drifting, which is discussed in section 5. However, in the case of mode C and D the low frequency feature was seen in the fluctuation spectra. In certain sections of these modes clear low frequency peaks could be clearly seen. In figure 6 we show two examples of the Longitude Resolved Fluctuation Spectra (LRFS, Backer 1970, 1973) corresponding to mode C (left panel), between pulse number 2142 and 2397, and mode D (right panel), between pulse number 2618 and 2873. The presence of low frequency feature is clearly

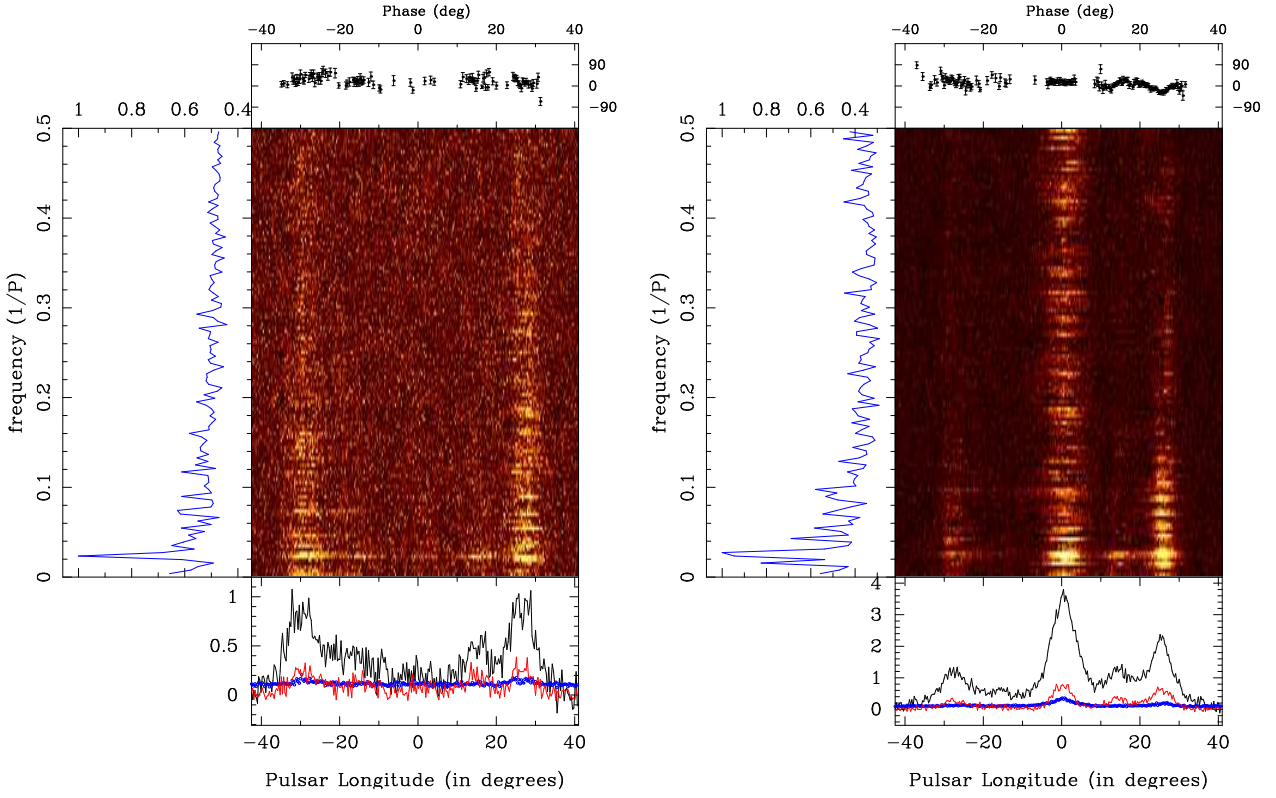


**Figure 6.** The figure shows the Longitude Resolved fluctuation spectra (LRFS) for two separate pulse sequences of the pulsar J2006–0807. The left panel corresponds to the sequence between pulse number 2142 and 2397, which belongs to mode C. The right panel shows an equivalent plot between pulse number 2618 and 2873, when the pulsar is in mode D. The central window shows the variation of the fluctuation spectra across the different longitudes. The bottom window shows the average profile from the pulses used for the spectra (black line). The bottom window also shows the variation of the peak amplitude across the pulse window (red line) along with the  $3\sigma$  baseline level of the LRFS along each longitude (blue dotted line). The left window shows the average LRFS across all longitudes and clearly indicates the presence of low frequency periodicity in both modes. The top window plots the phases across each longitude corresponding to all significant peak amplitudes greater than the baseline level. The phases show very little variations across the pulse window.

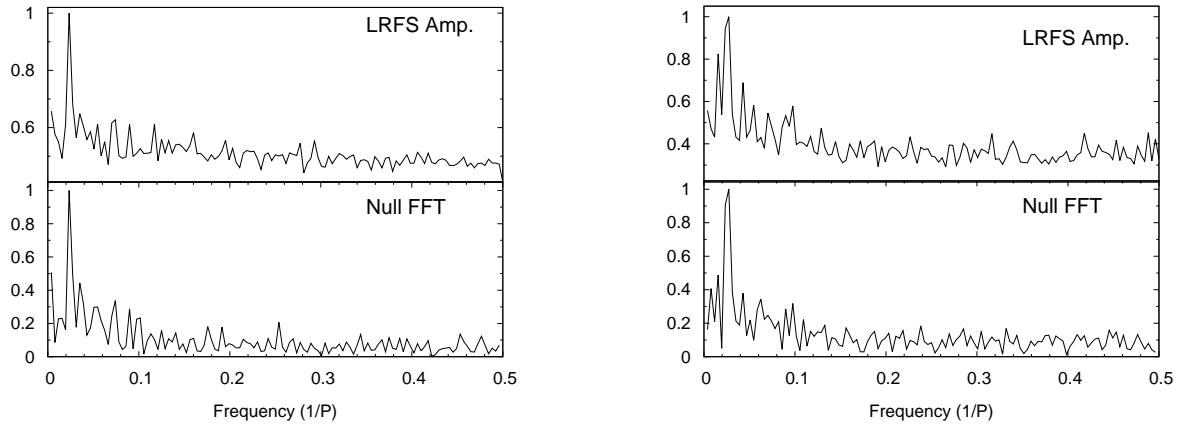


**Figure 7.** The figure shows a comparison between the longitude averaged amplitude of the Longitude Resolved Fluctuation spectrum (LRFS) of a pulse sequence and the spectra of the Fourier transform of the 0/1 series, with 0 corresponding to any null pulse and 1 corresponding to the burst pulse, for the same sequence. The left panel covers the pulse range 2142 and 2397, and belongs to mode C of PSR J2006–0807. The right panel is constructed for the pulse sequence between 2618 and 2873 periods and belongs to mode D. The low frequency peak is seen to be identical in both the spectra for each mode, which suggests that the low frequency structure in the LRFS originates due to nulling.

**Table 3.** Summary of Nulling in PSR J2006–0807

NF (%)	$\eta$	$N_T$	$\langle BL \rangle$ (P)	$\langle NL \rangle$ (P)	$P_N$ (P)
$28.6 \pm 3.4$	2577.5	262	8.3	9.8	$41.3 \pm 4.2$

seen. The modulations responsible for these feature are not due to drifting but are periodic amplitude modulations. This is clearly demonstrated by the phase variations, shown in the top window of each plot, which are relatively flat and featureless across the entire window. In a number of pulsars the low frequency features have now been shown to be a result of periodic nulling (Basu *et al.* 2017). To investigate this possibility we carried out an analysis similar to Basu *et al.* (2017), where a sequence of ‘0’ and ‘1’ were generated corresponding to the null and burst pulses respectively, and Fast Fourier Transforms (FFT) of these sequences were carried out. In figure 7 we show the results of this exercise for the two sequences belonging to mode C and D, described earlier, and compare the low frequency features with the longitude average LRFS for these sequences. The figure shows that these two features are identical, which suggests, that during certain instances the pulsar exhibit periodically varying nulling states. The periodic nulling is primarily seen during modes C and D, and is absent during the other modes two modes. Due to the frequent mode transitions and presence of long duration nulls, the low frequency feature becomes diffuse and indistinguishable from the boundary in the time average fluctuation spectra. The periodicity of the feature, when clearly seen, is  $P_N = 41.3 \pm 4.2 P$ . The presence of low frequency features associated with nulling, and the presence of drifting in the same system, has now been detected in eight pulsars, including J2006–0807 (Basu *et al.* 2017; Basu & Mitra 2018b). However, this is the first case where we have been able to show the periodic nulling clearly in the presence of core emission, where the core and cone nulls simultaneously.

In Table 3 we have summarized the nulling behaviour in this pulsar. The Table lists the total nulling fraction (NF) over all the observations, the reduction in intensity during nulling, specified by  $\eta$ , the number of transitions between null and burst sequences ( $N_T$ ), the average null ( $\langle NL \rangle$ ) and burst lengths ( $\langle BL \rangle$ ), and the periodicity ( $P_N$ ) of the nulling pattern during certain sections of pulse sequence.

#### 4 POLARIZATION BEHAVIOUR : EMISSION GEOMETRY

In our latest observations at 339 MHz we were unable to measure the polarized single pulses. Hence, we could not explore the polarization properties of the different emission modes in great detail. However, we have used the 333 MHz, MSPES observations to estimate the average polarization behaviour. As mentioned in section 2 the MSPES was not sensitive enough for polarized single pulses and we could only explore the average polarization behaviour. The survey recorded all the four stokes parameters (I, Q, U, V) for the pulsar. In figure 8 we show the average polarization behaviour corresponding to the average profile (left window), the mode B (middle window) and mode D (right window). We were unable to detect sufficient number of single pulses in the modes A and C to form

stable average profiles. The figure shows the average and modal profiles as well as the average linear ( $L = (Q^2 + U^2)^{0.5}$ ) and circular (V) polarization measurements. Table 4 shows the percentage of linear and circular polarization for the average profile as well as the two modes. We have calculated the percentage polarization, as a ratio between the linear and circular polarization with the total intensity, for the entire pulse window as well as the five individual components. The ratios were estimated as  $\langle L(\psi) \rangle / \langle I(\psi) \rangle$  and  $\langle V(\psi) \rangle / \langle I(\psi) \rangle$ , respectively, where  $\psi$  represents any specific longitude. The average linear polarization in all three cases were around 30%. However, this varied considerably across the different components. The core emission showed around 40% linear polarization in both the emission modes. The sign changing circular polarization was also seen for this component which is consistent with the core behaviour (Rankin 1990). The polarization was significantly lower in the first component, with mode B showing around 14% linear polarization and mode D around 9%. The inner cones, comprising of the second and fourth components, had significantly higher polarization, similar to the core, in both modes. The fifth component, on the other hand, had slightly lower polarization of around 25% in mode B and 18% in mode D, which was still higher than the leading component.

In addition, we have also estimated the polarization position angle (PPA) which are shown in the bottom panel of figure 8, for all three cases. The PPA usually shows a S-shaped curve, as seen in the figure, and is interpreted using the rotating vector model (RVM, Radhakrishnan & Cooke 1969), where the line of sight traverses diverging magnetic field lines. The PPA also shows the presence of two orthogonal polarization modes (Gil & Lyne 1995; Mitra *et al.* 2009), which are offset by  $90^\circ$  in phase, and are believed to be associated with the X and O modes of the emitting plasma waves (Melikidze *et al.* 2014; Mitra 2017). We were not able to explore the orthogonal modes from the single pulses but the average PPA showed signatures of the orthogonal modes. Mode B showed a typical S-shaped curve which closely followed the RVM. However, mode D showed significant departure from the RVM nature suggesting the presence of orthogonal modes. The deviation is seen primarily in the core component which is more prominent in this mode. The above behaviour suggests interesting associations between the emission modes and orthogonal polarization moding in this pulsar. Similar behaviour associated with the core component has also been reported during the different modes of PSR B1237+25 (Smith *et al.* 2013). This has interesting implications on the pulsar magnetospheric conditions during mode changing phenomenon and requires more sensitive studies of polarized single pulses from PSR J2006–0807.

The measurement of the profile widths, as well as the presence of average PPA estimates, make it possible to investigate the emission geometry. The geometry is usually characterised by two quantities,  $\alpha$ , which represents the angle between the rotation and magnetic axis of the pulsar, and  $\beta$ , the angle between the line of sight and rotation axis during their closest approach. It has been shown that in pulsars with a central core component,  $\alpha$  is related to the core width,  $\sin \alpha = W_b P^{-0.5} / W^c$ , where  $W^c$  is the core width measured at 50% level of peak intensity, and  $W_b$  corresponds to the lower boundary of the distribution of the core widths with period (Rankin 1990). The core boundary width have recently been measured to be  $W_b = 2.39 \pm 0.26^\circ$ , at 333 MHz, by Skrzypczak *et al.* (2018). The angles  $\alpha$  and  $\beta$  can also be estimated from the RVM fits to the PPA. However, these fits yield values which are highly correlated and are not effective in estimating the emission geometry (Everett & Weisberg 2002;

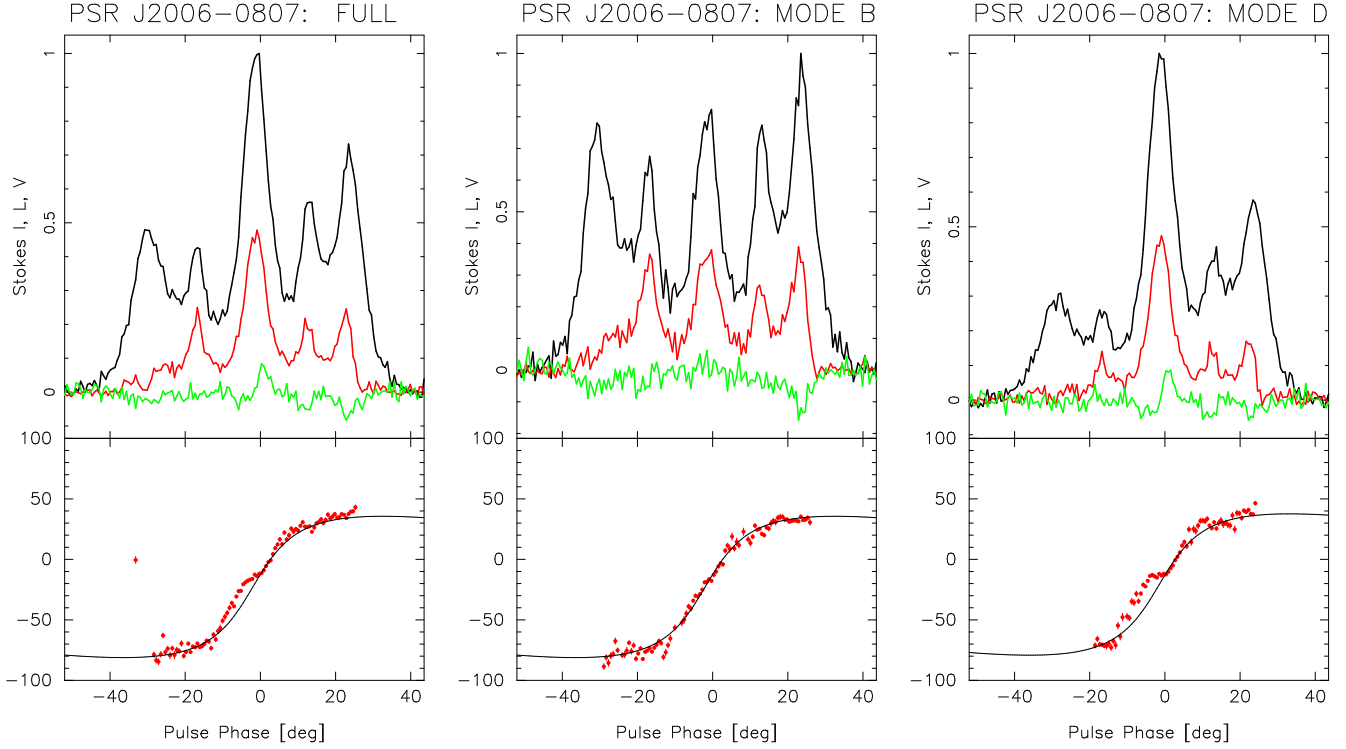


**Figure 8.** The figure shows the average polarization properties of the pulsar J2006–0807 using the MSPES, 333 MHz observations (Mitra *et al.* 2016). Due to the lower sensitivity and shorter duration of these observations we could only obtain sufficiently sensitive studies of two emission modes, mode B and mode D. The left panel corresponds to the average over the full observing session, the middle panel shows mode B and right panel represents the behaviour of mode D. The top window of each plot shows the average profile (black line) along with the linear polarization (L, red line) and the circular polarization (V, green line). The bottom window in each figure shows the polarization position angle (PPA). The figure also shows the rotating vector model (RVM) fits to the PPA, where the RVM fits have been estimated from PPA of mode B.

**Table 4.** The polarization properties of PSR J2006–0807

	Type	Longitude Range		AVG. PROFILE		MODE B		MODE D	
				%(L/I)	%(V/I)	%(L/I)	%(V/I)	%(L/I)	%(V/I)
Full Window	—	-40.3°	34.2°	29.86±0.02	-2.93±0.03	30.29±0.03	-6.06±0.05	28.23±0.03	-1.79±0.04
Component I	Outer Cone	-40.3°	-22.0°	12.20±0.09	-4.7±0.1	13.8±0.1	-7.0±0.2	9.3±0.2	-2.8±0.3
Component II	Inner Cone	-21.4°	-10.4°	41.7±0.2	-1.7±0.2	47.0±0.2	-5.7±0.3	33.8±0.3	0.7±0.5
Component III	Core	-9.8°	7.3°	40.91±0.06	1.23±0.08	42.2±0.1	-0.4±0.2	39.51±0.07	0.6±0.1
Component IV	Inner Cone	7.9°	17.1°	31.1±0.1	-5.7±0.2	30.5±0.2	-6.6±0.3	27.7±0.2	-5.1±0.3
Component V	Outer Cone	17.7°	34.2°	20.92±0.08	-5.6±0.1	25.0±0.1	-10.4±0.2	17.7±0.1	-4.5±0.2

Mitra & Li 2004). However, the steepest gradient ( $R_{PPA}$ ) of the PPA is related to the two angles,  $R_{PPA} = \sin\alpha/\sin\beta$ , and provides a more reliable estimate. Once, the geometrical angles are known, the opening angle ( $\rho$ ) of the emission beam can also be estimated from the separation between the inner and outer conal component pairs using principles of spherical geometry (Gil *et al.* 1984),  $\cos\rho = \cos\beta - 2\sin\alpha \sin(\alpha+\beta) \sin^2 W_{sep}/4$ .

In Table 5 we have estimated the emission geometry for the average profile as well as the different emission modes. The Table

shows the estimated core widths at 50% level of peak intensity, the separation between the peaks of the inner ( $W_s^{in}$ ) and outer conal ( $W_s^{out}$ ) pairs, as well as the estimated  $\alpha$  from the core width. In order to estimate  $\beta$  we calculated  $R_{PPA} = 4.6 \pm 0.2^\circ/\rho$ , using the PPA of mode B which showed least deviations from the RVM. The  $\beta$  for all the modes are shown in the Table along with the  $\rho$  for the inner and outer cones. The RVM fits shown in figure 8 were estimated from the geometry reported in Table 5. In case of mode C the core component was not prominent and hence the geometry could not be estimated. However, we calculated the opening angles for the conal

**Table 5.** Estimating the emission geometry of PSR J2006–0807

	$W_{50}^{core}$ ( $^{\circ}$ )	$W_s^{in}$ ( $^{\circ}$ )	$W_s^{out}$ ( $^{\circ}$ )	$\alpha$ ( $^{\circ}$ )	$\beta$ ( $^{\circ}$ )	$\rho_{in}$ ( $^{\circ}$ )	$\beta/\rho_{in}$	$\rho_{out}$ ( $^{\circ}$ )	$\beta/\rho_{out}$
Avg. Profile	$8.2 \pm 0.9$	$29.7 \pm 0.9$	$54.0 \pm 0.9$	$22.4 \pm 5.2$	$4.7 \pm 1.0$	$7.8 \pm 0.2$	0.60	$12.1 \pm 0.6$	0.39
Mode A	$7.9 \pm 0.9$	$29.3 \pm 0.9$	$53.1 \pm 0.9$	$23.5 \pm 5.6$	$4.9 \pm 1.1$	$8.0 \pm 0.3$	0.61	$12.5 \pm 0.6$	0.39
Mode B	$8.2 \pm 0.9$	$30.2 \pm 0.9$	$54.0 \pm 0.9$	$22.5 \pm 5.2$	$4.7 \pm 1.0$	$7.9 \pm 0.3$	0.59	$12.2 \pm 0.6$	0.39
Mode C	—	$31.1 \pm 0.9$	$58.0 \pm 0.9$	—	—	$8.0 \pm 0.3$	—	$12.9 \pm 0.7$	—
Mode D	$8.2 \pm 0.9$	$29.7 \pm 0.9$	$53.5 \pm 0.9$	$22.4 \pm 5.2$	$4.7 \pm 1.0$	$7.8 \pm 0.2$	0.60	$12.0 \pm 0.6$	0.39

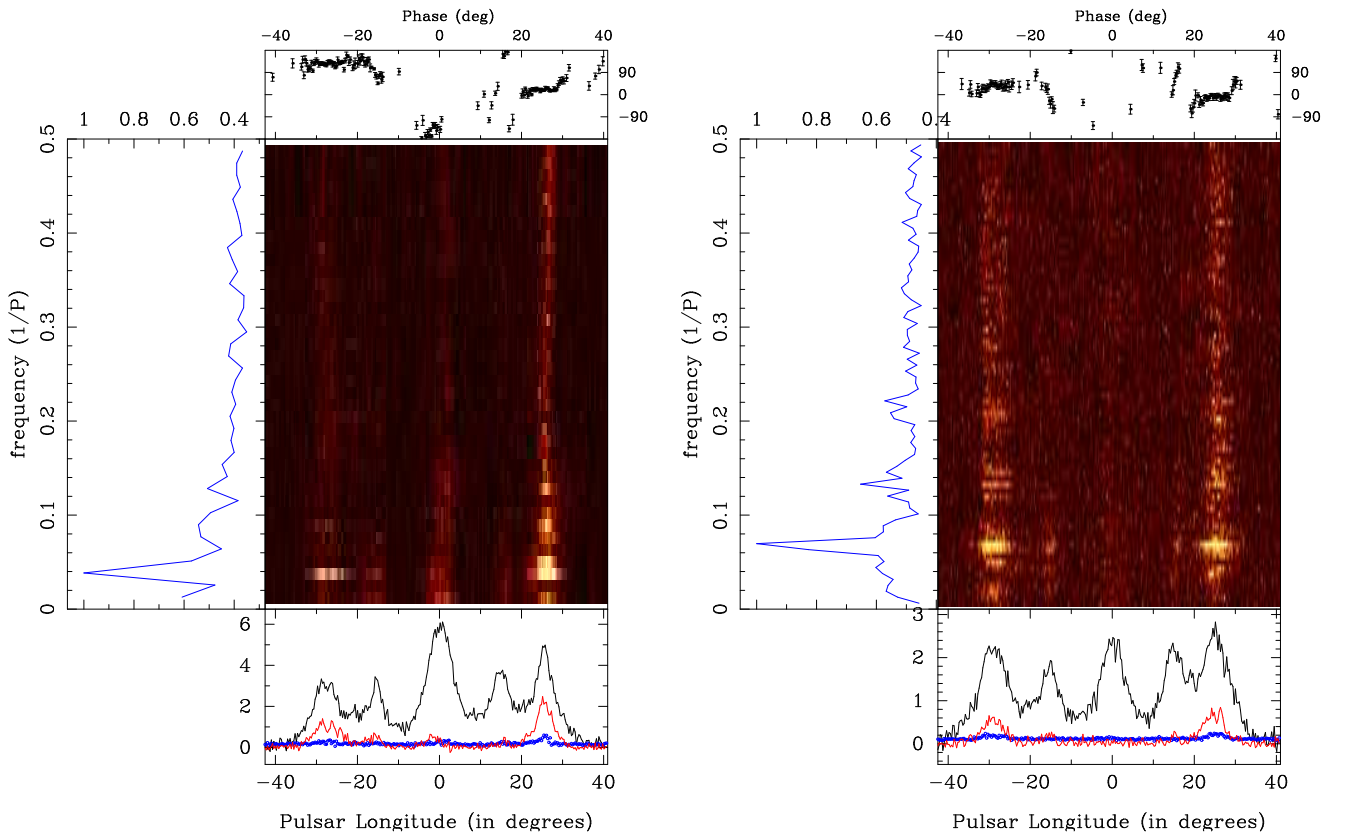


**Figure 9.** The figure shows the Longitude Resolved fluctuation spectra (LRFS) for two separate pulse sequences of the pulsar J2006–0807. The left panel corresponds to the sequence between pulse number 1716 and 1793, which belongs to mode A. The right panel shows an equivalent plot between pulse number 697 and 855, when the pulsar is in mode B. The subpulse drifting is seen in both modes with different periodicities. The phase variations are also shown in the top window, and shows clear evolution between the inner and outer cones. The lower window shows the average profile formed from the pulses used for the LRFS estimates in each case (black lines). The bottom window also shows the variation of the amplitude of the peak frequency across the pulse window (red line) as well as  $3\sigma$  level of the baseline of the LRFS for each pulse longitude (blue dotted line).

separation using average geometry. The pulsar geometry gives similar values for the different emission modes. Our estimates of  $\alpha$  were different from the previous measurement of Rankin (1993b) who reported a value of  $\alpha=13^{\circ}$ . This primarily results from the estimate of the core width, which was  $14^{\circ}$  in the previous work, and significantly larger than our measurements. We examined the high frequency ( $> 1$  GHz) profiles available for this pulsar, from the archival observations, and it was found that the core was not clearly separated from the conal emission at higher frequencies. This can

possibly lead to a larger estimate. It is also possible that the pulsar widths have undergone an absorption at lower frequencies leading to narrower measurements (Rankin 1983). This will require more detailed observations particularly at frequencies above 1 GHz.

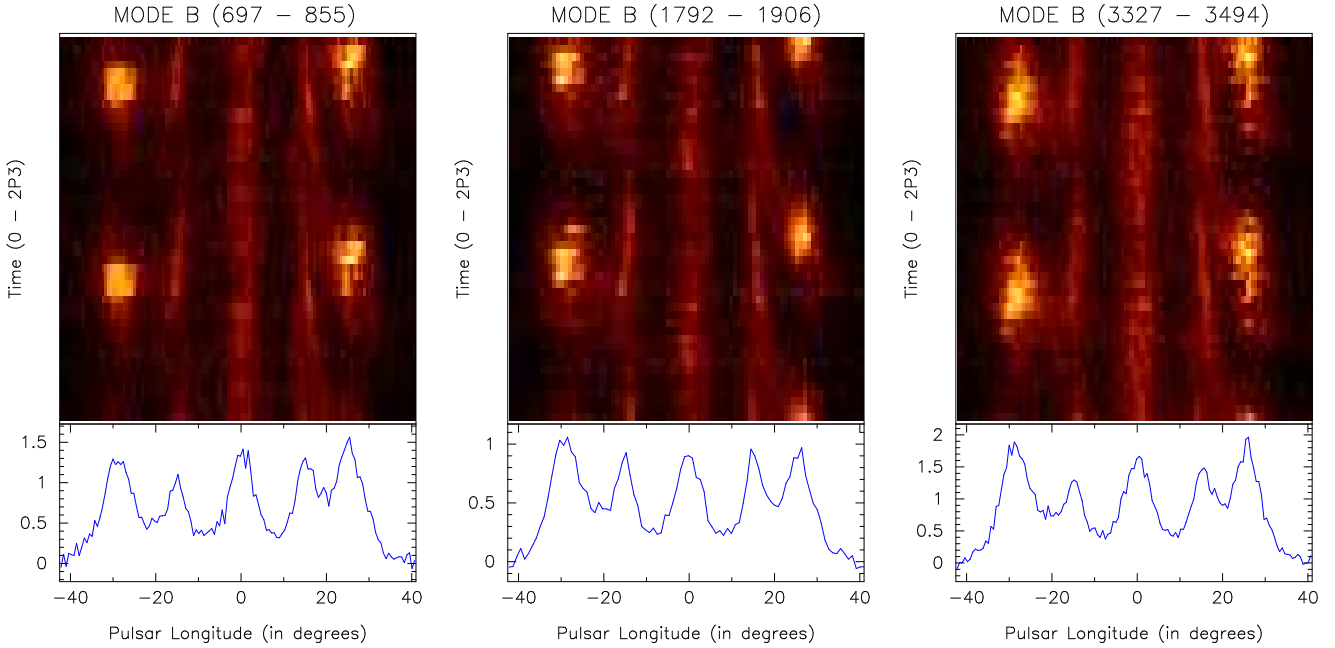


**Figure 10.** The figure shows  $P_3$  folded profile during emission mode B for three different sections, between pulse 697 and 855 (left panel), between pulse 1793 and 1907 (middle panel) and from pulse 3327 to 3494 (right panel). In order to present a full outline of the subpulse tracks the same profile have been stacked on top to give a  $2P_3$  range along the y-axis. The outer cones show bright spots indicating phase stationary drifting. The inner cones show extended tracks indicating large phase variations. The direction of these tracks have opposite sense which is suggestive of bi-drifting nature.

**Table 6.** Subpulse Drifting in PSR J2006–0807

Pulse	Mode	$f_p$ ( $cy/P$ )	FWHM ( $cy/P$ )	S	$P_3$ ( $P$ )
100 - 160	A	$0.0342 \pm 0.0107$	0.0252	24.0	$29.3 \pm 9.2$
616 - 674	A	$0.0337 \pm 0.0136$	0.0320	13.7	$29.7 \pm 12.0$
697 - 855	B	$0.0667 \pm 0.0054$	0.0128	40.5	$15.0 \pm 1.2$
1716 - 1793	A	$0.0390 \pm 0.0071$	0.0166	36.8	$25.6 \pm 4.6$
1793 - 1907	B	$0.0699 \pm 0.0039$	0.0092	60.8	$14.3 \pm 0.8$
2030 - 2123	A	$0.0371 \pm 0.0107$	0.0252	20.1	$27.0 \pm 7.8$
3233 - 3304	A	$0.0338 \pm 0.0107$	0.0253	20.7	$29.6 \pm 9.4$
3327 - 3494	B	$0.0657 \pm 0.0035$	0.0082	76.3	$15.2 \pm 0.8$
4188 - 4240	B	$0.0675 \pm 0.0184$	0.0434	8.5	$14.8 \pm 4.0$
4702 - 4798	A	$0.0367 \pm 0.0098$	0.0231	20.2	$27.3 \pm 7.3$

## 5 SUBPULSE DRIFTING

We have carried out a detailed analysis of the subpulse drifting seen in the emission modes A and B. The drifting analysis was particularly challenging, firstly because of the mixture of drifting and non-drifting modes in the pulse sequence, and secondly because there was no clear boundary between the modes A and B.

As mentioned earlier in section 3.1, we have visually inspected the entire single pulse sequence to identify the modes A and B and investigated the nature of subpulse drifting. We have measured the LRFS of individual pulse sequences in the two modes. Two typical examples of LRFS are shown in figure 9, where the left panel corresponds to a sequence between pulse range 1716 and 1793 in mode A, and the right panel shows the LRFS for a sequence in mode B between pulses 697 and 855. The peak frequency corresponding to drifting periodicity is seen primarily in the conal components, with the outer cones being most prominent. The core component either showed a low level intensity (mode A) or drifting was completely absent (mode B). In addition the phase variations corresponding to the peak frequency (top window in figure 9) also show significant evolution across the different components. The figure also shows the errors in phase values which were computed as :

$$\delta\phi = \frac{|x\delta y - y\delta x|}{x^2 + y^2}; \quad \text{where } x = \text{Re}(I_\nu), \quad y = \text{Im}(I_\nu),$$

where  $\delta x$  and  $\delta y$  have been computed from the baseline rms of the real and imaginary parts of the spectral power at horizontal bins corresponding to the peak drifting frequency ( $f_p$ ).

The phase behaviour provides a clear distinction between subpulse drifting and other periodic phenomenon like periodic nulling or amplitude modulation (see figure 6). In both emission modes the phases corresponding to the outer cones are relatively flat, which transitions to large variations for the inner cones. In order to further explore the phase variations we have carried out  $P_3$  folding for all drifting sequences. In most of these cases the number of pulses were not adequate to form a stable profile. However, in a few cases, in mode B, we could establish the subpulse behaviour from the  $P_3$  folded profiles. In figure 10, the  $P_3$  folded profile for three sequences have been shown, pulses 697 and 855 (left panel), between

**Table 7.** Slope of the drifting phase variations in the inner cones

Pulse	Mode	$d\phi/d\psi$ ( $^\circ/P$ )	
		COMP 2	COMP 4
697 - 855	B	$-32.7 \pm 5.7$	$65.6 \pm 7.6$
1716 - 1793	A	$-31.1 \pm 5.0$	$58.2 \pm 6.1$
1793 - 1907	B	$-42.9 \pm 5.0$	$75.5 \pm 5.9$
2030 - 2123	A	$-40.5 \pm 6.2$	$56.5 \pm 5.5$
3233 - 3304	A	$-45.7 \pm 4.4$	$76.4 \pm 5.3$
3327 - 3494	B	$-25.1 \pm 2.8$	$66.6 \pm 5.6$

pulse 1793 and 1907 (middle panel) and from pulse 3327 to 3494 (right panel). The outer cones are seen as bright spots which are indicative of their phase stationary nature. The inner cones on the other hand show extended tracks which suggest large phase variations. Additionally, these tracks are in opposite directions with the second component showing a positive drifting and fourth component with negative drifting. This behaviour is also seen in the fluctuation spectra phase and is indicative of the rare phenomenon known as bi-drifting, where the subpulse drifting in different components have opposite directions (Champion *et al.* 2005).

The drifting in modes A and B have different periodicities, with mode A showing a much lower frequency peak compared to mode B in the fluctuation spectra. In Table 6 we report all the sections in the pulse sequence where a clear drifting peak could be measured from the LRFS. In each case we have also estimated the S factor, which is defined as the ratio between peak height and Full Width at Half Maximum (FWHM) of the feature, and gives a measure of the peak strength. The Table lists the pulse range corresponding to each measurement along with emission mode,  $f_p$ , FWHM of each feature, S factor, and drifting periodicity ( $P_3$ ) in units of rotation period ( $P$ ). The error in the peak frequency is estimated as  $\text{FWHM}/2\sqrt{2\ln(2)}$ , where  $2\sqrt{2\ln(2)}$  is the scaling for gaussian approximation (Basu *et al.* 2016). The Table reports six pulse sequences in mode A with a mean  $P_3$  of  $27.1 \pm 8.9 P$ . Additionally, four sequences in mode B are also reported with a mean  $P_3$  value of  $14.8 \pm 0.3 P$ . Within measurement errors the drifting periodicity during mode A is roughly two times that of mode B. In order to explore any harmonic relationship between the two we have investigated the phase behaviour of the inner conal components for the different sequences where the phase variations could be clearly distinguished in the LRFS. A linear approximation to the phase variations for each sequence was estimated and the phase gradient ( $d\phi/d\psi$ ) is reported in table 7. The gradients in the two conal components are of opposite signs consistent with the bi-drifting behaviour and the magnitude is higher for the fourth component compared to the second component. If the periodicities during the two modes are harmonically related then for each component the phase gradient during mode B (first harmonic) should be a factor of 2 greater than the gradient in mode A. No, such dependence is seen in the phase behaviour during the two modes which rules out any harmonic dependence between the two.

We have also investigated the nature of subpulse drifting in the individual components and whether any low level drifting is seen

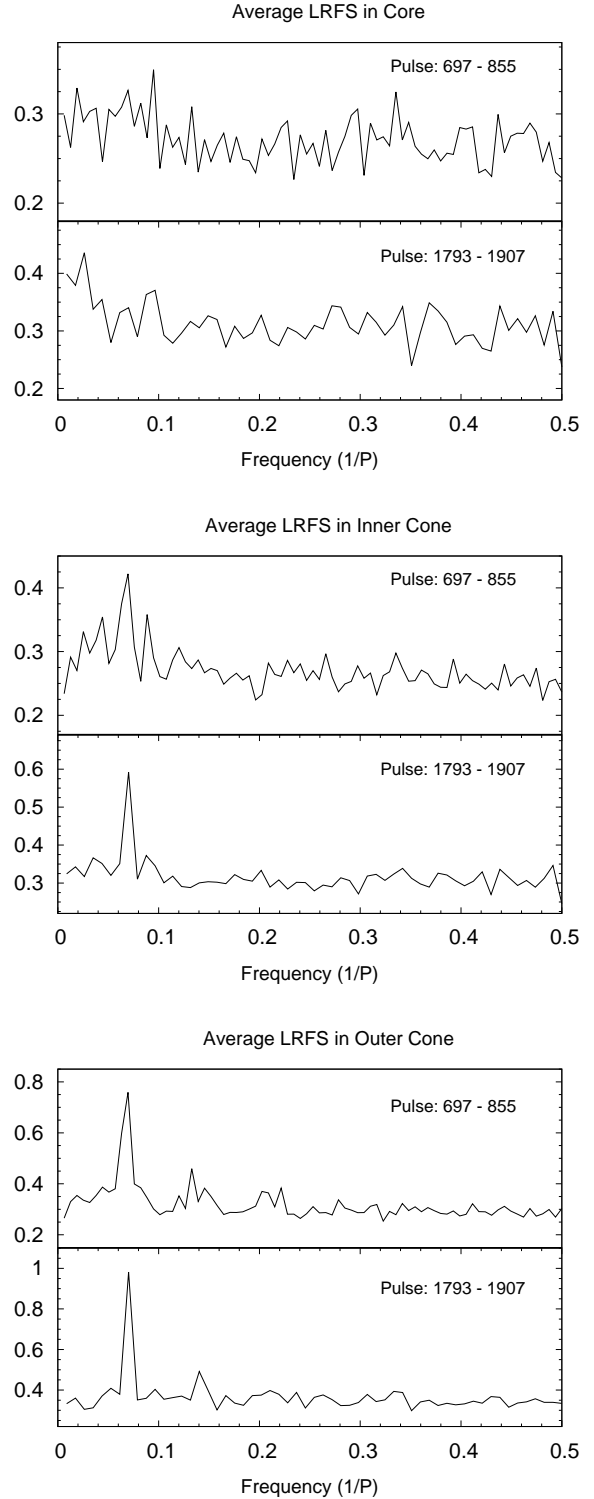


**Figure 11.** The figure shows the Longitude Resolved Fluctuation Spectra (LRFS) averaged across the core (top panel), inner cone (middle window) and outer conal (bottom window) components, during two intervals in mode B. The top panel corresponds to the pulses between 697 and 855, while the bottom panel corresponds to pulse range 1793 and 1907. The periodicity corresponding to drifting is clearly seen in the inner and outer conal components. However, no clear drifting feature is visible in the core component.

in the core component. In figure 11 we show the average LRFS for the core (top window), inner cones (middle window) and the outer cones (bottom window), for two pulse ranges between 697 and 855 (top panel in each window) and between pulses 1793 and 1907 (bottom panel), when the pulsar was in mode B. The presence of prominent drifting peaks is seen for the inner and outer cones. However, no such features are seen for the core component demonstrating the absence of drifting in the core. However, there is a possible low level, wide structure present at the lower frequencies. This is likely due to the presence of periodic amplitude modulations in these modes in addition to drifting. However, these structures cannot be related to the sharp low frequency features seen in modes C and D in section 3.2 as a result of nulling, since no periodic nulling is seen in during these modes.

## 6 DISCUSSION

### 6.1 The interaction between Nulling and Mode changing

The single pulses in PSR J2006–0807 show large diversity with four distinct emission modes, two of which show subpulse drifting, in addition to long intervals of nulling. There are only a few known pulsars which exhibit more than two emission modes along with subpulse drifting. The most well studied pulsar in this group is PSR B0031–07 with three distinct drifting modes (Vivekanand & Joshi 1997; Smits *et al.* 2005; McSweeney *et al.* 2017). The pulsar also shows the presence of long duration periodic nulls (Basu *et al.* 2017). It has a conal profile and belongs to the  $S_d$  profile class. Other examples include the pulsars B1819–22 (Basu & Mitra 2018b), B1918+19 (Rankin *et al.* 2013), J1944+17 (Kloumann & Rankin 2010) and B2319+60 (Wright & Fowler 1981). The pulsar B1819–22 has a conal double profile and exhibit two distinct drifting modes in addition to a non-drifting state. The pulsar also shows short duration nulls during all emission states which are periodic in nature. In case of PSR B1918+19 there are three distinct drift modes and an additional disordered mode. The pulsar also shows the presence of nulling which is periodic. The pulsar has a conal profile belonging to the  $cT$  class. The pulsar B1944+17 also has a  $cT$  profile and nulls for around 70% of the time. In the burst state the pulsar shows the presence of four modes, three of which show subpulse drifting. The nulling can be divided into two categories, short duration nulls in between the burst states which likely showed low level emission, and long duration nulls lasting up to 300 periods. The presence of periodicity was detected associated with the long duration nulls (Basu *et al.* 2017). Finally, the pulsar B2319+60 shows the presence of three drifting modes and nulls for roughly 30% of the time. There is no study demonstrating the periodicity of the nulls in this case, however, the fluctuation spectra shows the presence of a low frequency feature which maybe associated with nulling. The pulsar profile has four conal components and belongs to the  $cQ$  class. All the previously reported pulsars showing multiple mode changing along with subpulse drifting are associated with conal profiles. On the contrary the pulsar J2006–0807 has five components, including a central core component, and belongs to the M profile class. This is the first case where we have found multiple mode changing, drifting and nulling in the presence of the core emission. As a result we can conclude that such phenomenon are not restricted to conal pulsars alone and no preferred line of sight geometrical configuration is responsible for such systems.

There is no clear boundary of transition between the two drift-

ing modes A and B which is also unique to this pulsar. A gradual shift in the drifting periodicity was reported for the pulsar B0943+10 (Backus *et al.* 2011). The variation was small and seen in the Burst mode as an exponential decay over timescale of few hours. There was no separate mode identification carried out for this evolution in drifting. In the case of PSR B0809+74 which shows systematic drifting, a null associated mode changing has also been reported (van Leeuwen *et al.* 2002). The drift rate shows a gradual variation lasting several hundred periods after certain intervals of nulls, before transitioning to the earlier mode. There is no clear boundary during the mode transition which lasts for around 20  $P$ . Similarly, the evolution between modes A and B in PSR J2006–0807 occurs over 10-20  $P$  with distinct evolution in drifting periodicity as well as profile shape. The pulsar also shows the presence of two types of nulls, the short duration nulls in between the burst states in the non-drifting modes, as well as longer duration nulls lasting up to 100  $P$ . This behaviour is different from the other cases where the short nulls are present between both the drifting and non-drifting modes. Additionally, only the short duration nulls in the non-drifting modes show clear periodicity. This clearly distinguishes the two phenomenon which was not apparent in previous cases. The presence of periodic nulling is reported in around twenty pulsars (Herfindal & Rankin 2009; Basu *et al.* 2017). In this group there are seven pulsars which show presence of both mode changing and periodic nulling, including the six pulsars discussed in this section. In recent works (Basu *et al.* 2016; Mitra & Rankin 2017; Basu *et al.* 2017; Basu & Mitra 2018a,b) a clear distinction has been between the different periodic phenomenon in pulsars. The subpulse drifting has different physical properties compared to periodic nulling and periodic amplitude modulations. This is highlighted by the dependence of the respective periodicities with  $\dot{E}$ . Additionally, it has also seen that the subpulse drifting is strictly a conal phenomenon while the nulling and mode changing affects all the components, both core and cones, at the same time.

### 6.2 Periodic Nulling in presence of Core component

As discussed above the pulsar shows the presence of periodicity associated with nulling as well as subpulse drifting. This is the eighth case where the presence of subpulse drifting and periodic nulling were seen in the same system (Basu *et al.* 2017; Basu & Mitra 2018b). However, this is the first time that we have clearly seen periodic nulling in the presence of the core component, where the core and cone nulls simultaneously. Our analysis provides conclusive proof that the periodic nulling is a separate phenomenon, completely different from subpulse drifting. Firstly, the two phenomena were seen in different emission modes with contrasting single pulse behaviour. The subpulse drifting was seen in the emission modes A and B where no significant nulling was seen, while the periodic nulling was observed in the modes C and D where no systematic drift pattern was visible. Secondly, the drifting was seen as subpulse variation affecting each component differently, while the periodic nulling affected the entire single pulse, with either the presence or absence of emission across the pulse window. This was also reflected in the phase behaviour, with the phases being completely flat across the pulse window during periodic nulling, while they showed significant structure during drifting. Finally, the behaviour of the core emission clearly demonstrated the difference between the two. While the core and the cones nullled simultaneously during periodic nulling, the subpulse drifting was absent in the core component. The two phenomenon have been understood in the past (Herfindal & Rankin 2009) in terms of

the carousel model (Ruderman & Sutherland 1975; Gil & Sendyk 2000; Deshpande & Rankin 2001), where the emission beam was expected to consist of circulating beamlets which were responsible for subpulse drifting. The longer periodicity associated with periodic nulling was interpreted as a circulation time,  $P_4$ , of each beamlet around the emission beam. The periodic nulls were either LOS traverse between empty regions of the circulating pattern or corresponded to missing or weak beamlets (Rankin *et al.* 2013). Basu *et al.* (2016, 2017) found that subpulse drifting was seen in pulsars with spindown energy loss ( $\dot{E}$ )  $< 10^{33}$  erg s $^{-1}$ , while no such restriction appeared for periodic nulling and low frequency amplitude modulations. Additionally,  $P_3$  was found to be inversely correlated with  $\dot{E}$ , while no such dependence was seen for  $P_N$ . In a more recent work investigating subpulse drifting, Basu *et al.* (2019) established subpulse drifting to be primarily a conal phenomenon, while periodic amplitude modulation and periodic nulling were associated with the entire pulse window. As a result these studies claimed different physical processes to be responsible for subpulse drifting and periodic nulling. Our analysis for PSR J2006–0807, presented in this work, provides further and more conclusive evidence to support this claim.

### 6.3 Understanding the Drifting Behaviour

One of the most striking feature about the pulsar’s single pulse behaviour is the nature of subpulse drifting seen across the pulse window. The central line of sight traverse of the emission beam provides a wide window into the drifting process and have given us improved insights into the inner cones of a M type profile class. The fluctuation spectral studies of drifting give measurements of drifting periodicity as well as phase variations corresponding to subpulse motion across each component in the pulsar profile. As reported in section 5 the phase variations are very different for the inner and outer cones. The outer cones were mostly phase stationary with less than 50° variations across each component. On the other hand the inner cones, particularly in mode B, showed large variations in excess of 100° across each component. A recent survey of subpulse drifting was conducted by Basu *et al.* (2019), where the phenomenon, seen in around 60 pulsars, was classified into four groups based on their phase behaviour. A connection between the phase variations and profile class, and as an extension emission geometry, was seen. The drifting in pulsars with a central core component were classified as ‘Low-mixed’ phase modulated drifting. It was previously expected that the subpulse drifting in central LOS traverse, associated with core emission, was phase stationary (Rankin 1986). However, Basu *et al.* (2019) noted that certain pulsars, like PSR B1237+25, had indications of considerable phase variations, particularly for the inner conal components. The indications for such phase behaviours in PSR B1237+25 was also seen in Rankin & Ramachandran (2003). No detailed drifting phase measurements were available for PSR J2006–0807, but the pulsar was also classified in the ‘Low-mixed’ category. The phase behaviour in both modes A and B, reported here, is consistent with this classification. To the best of our knowledge this is the first pulsar where we have conclusively found large phase variations in a system with a core component. It is possible that the phase behaviour seen for the inner and outer cones are more common in the M type profiles, as also indicated in B1237+25 (see the phase plots in Basu *et al.* 2019). Detailed observations exploring the drifting phase behaviour in other such pulsars is required to explore this further.

In addition to large variations the phases also show opposite directions in the inner cones resulting in bi-drifting. This

is only the fourth known example of bi-drifting phenomenon, with the other three being J0815+0939 (Champion *et al.* 2005; Szary & van Leeuwen 2017), B1839–04 (Weltevrede 2016) and J1034–3224 (Basu & Mitra 2018a), which are all wide profile conal only pulsars. In PSR J0815+0939 there are four components in the profile which belongs to the  $c_Q$  class. The second component shows positive drifting while the other three has negative drifting. In PSR B1839–04 the profile has two components with opposite drifting directions. The pulsar J1034–3224 has four distinct conal components in addition to a precursor like emission (Basu *et al.* 2015). The phase variations are opposite in every alternate conal component of this pulsar. The bi-drifting phenomenon is difficult to understand using standard model of plasma generation in Inner Acceleration Region (IAR, Ruderman & Sutherland 1975, RS75). An usual circulation of sparks around the magnetic axis in a strictly dipolar polar cap cannot give drifting in opposite directions for any line of sight traverse of the emission beam. A number of models for a modified IAR has been proposed to explain the bi-drifting phenomenon. Qiao *et al.* (2004a,b) suggested the IAR to consist of an inner annular gap inside the traditional RS75 gap. The drift velocity has opposite directions in the two gaps which was used to explain the bi-drifting effect. However, as pointed out the drawback of this model is the requirement of different number of rotating sparks circulating at varying speeds in the two gaps to reproduce the observed drifting. An empirical model was proposed by Wright & Weltevrede (2017) where the emission beam was assumed to be elliptical and tilted with respect to the fiducial plane. It was shown that specialized line of sight traverses can sample the circulating pattern in a manner that the drifting in different components are reversed. A more physical model was suggested by Szary & van Leeuwen (2017), where the IAR was assumed to be dominated by non-dipolar fields. It was suggested that the sparks circulated around a point of maximum potential within the polar cap. This configuration reproduced the elliptical beams suggested by Wright & Weltevrede (2017), thereby explaining the bi-drifting phenomenon. The phase behaviour in PSR J2006–0807 is different primarily due to the presence of the core component which does not drift, and bi-drifting is only seen in the inner cones. This configuration also greatly constrains the line of sight geometry which is supposed to traverse the emission beam centrally. In addition to the bi-drifting in the inner cones, the outer cones exhibit almost phase stationary behaviour. Some phase variations are expected for pulsars with lower magnetic inclination angles even for central line of sight traverse. However, the difference in the phase behaviours of the inner and outer cones cannot simply be explained by a low inclination angle. In contrast to the widely varying phase behaviour across the pulse window the peak frequency corresponding to the drifting periodicity remains constant for all components. This implies that the drifting speed remains constant across the pulse window, despite the direction of motion having large variations as indicated by the phase behaviour. In addition to the pulsar J2006–0807, Basu *et al.* (2019) have also found that the drifting periodicity remains constant across the pulse window for all pulsars with systematic drift patterns, despite large phase variations.

## 7 SUMMARY

We have carried out a detailed single pulse analysis of the five component pulsar J2006–0807. The pulsar profile was characterised by a central core component surrounded by pairs of inner and outer cones. The single pulses revealed the presence of four distinct emis-

sion modes along with intervals of nulling. In two emission modes, A and B, the pulsar showed the presence of subpulse drifting, while the other two modes, C and D, did not drift, but were interspersed with periodic nulls. The pulsar spent roughly a third of its time in the two drifting modes, another third in the two non-drifting modes and the remaining in the nulling state. We have estimated the average polarization properties and emission geometry, which suggested that the emission location within the magnetosphere was unchanged for the different modes. Additionally, the polarization also indicated the presence of orthogonal moding which was connected with the mode changing phenomenon. The subpulse drifting showed diversity in the drifting behaviour across the different components, with the outer cones showing phase stationary drifting, the inner cones showing large phase modulated bi-drifting. The emission showed a gradual decrease in intensity as the pulsar transitioned from mode A to B. In addition, the fluctuation spectra also showed a low level wide structure at low frequencies during this emission state, primarily in the core component which was due to periodic amplitude modulation. The amplitude modulation was also likely to be present in the conal components but was hidden under the prominent drifting feature.

#### ACKNOWLEDGMENTS

We thank the referee for the comments which helped to improve the paper. DM acknowledges funding from the grant “Indo-French Centre for the Promotion of Advanced Research - CEFIPRA”. We thank the staff of the GMRT who have made these observations possible. The GMRT is run by the National Centre for Radio Astrophysics of the Tata Institute of Fundamental Research.

#### REFERENCES

- Backer, D.C. 1970, *Nature*, 228, 1297  
 Backer, D.C. 1973, *ApJ*, 182, 245  
 Backus, I.; Mitra, D.; Rankin, J.M. 2011, *MNRAS*, 418, 1736  
 Basu, R.; Mitra, D.; Rankin, J.M. 2015, *ApJ*, 798, 105  
 Basu, R.; Mitra, D.; Melikidze, G.I.; Maciesiak, K.; Skrzypczak, A.; Szary, A. 2016, *ApJ*, 833, 29  
 Basu, R.; Mitra, D.; Melikidze, G.I. 2017, *ApJ*, 846, 109  
 Basu, R.; Mitra, D. 2018a, *MNRAS*, 475, 5098  
 Basu, R.; Mitra, D. 2018b, *MNRAS*, 476, 1345  
 Basu, R.; Mitra, D.; Melikidze, G.I.; Skrzypczak, A. 2019, *MNRAS*, 482, 3757  
 Champion, D.J.; Lorimer, D.R.; McLaughlin, M.A.; *et al.* 2005, *MNRAS*, 363, 929  
 Deshpande, A.A.; Rankin, J.M. 2001, *ApJ*, 322, 438  
 Everett, J. E., Weisberg, J. M. 2001, *ApJ*, 553, 341  
 Gajjar, V.; Joshi, B.C.; Kramer, M. 2012, *MNRAS*, 424, 1197  
 Force, M.M.; Rankin, J.M. 2010, *MNRAS*, 406, 237  
 Gil, J.; Gronkowsky, P., Rudnicki, W. 1984, *A&A*, 132, 312  
 Gil, J.; Lyne, A. 1995, *MNRAS*, 276L, 55  
 Gil, J.; Sendyk, M. 2000, *ApJ*, 541, 351  
 Hankins, T.H.; Wolszczan, A. 1987, *ApJ*, 318, 410  
 Herfindal, J.L.; Rankin, J.M. 2007, *MNRAS*, 380, 430  
 Herfindal, J.L.; Rankin, J.M. 2009, *MNRAS*, 393, 1391  
 Kloumann, I.M.; Rankin, J.M. 2010, *MNRAS*, 408, 40  
 Maan, Y.; Deshpande, A.A. 2014, *ApJ*, 792, 130  
 Maciesiak, K.; Gil, J.; Melikidze, G.I. 2012, *MNRAS*, 424, 1762  
 McSweeney, S.J.; Bhat, N.D.R.; Tremblay, S.E.; Deshpande, A.A.; Ord, S.M. 2017, *ApJ*, 836, 224  
 Melikidze, G.I.; Mitra, D.; Gil, J.A. 2014, *ApJ*, 794, 105  
 Mitra, D., Deshpande, A.A. 1999, *A&A*, 346, 906  
 Mitra, D., Rankin, J.M. 2002, *ApJ*, 577, 322  
 Mitra, D., Li, X. H. 2004, *A&A*, 421, 215  
 Mitra, D.; Gil, J.; Melikidze, G. 2009, *ApJL*, 696, L141  
 Mitra, D.; Basu, R.; Maciesiak, K.; Skrzypczak, A.; Melikidze, G.I.; Szary, A.; Krzeszowski, K. 2016, *ApJ*, 833, 28  
 Mitra, D.; Rankin, J. 2017, *ApJ*, 468, 4601  
 Mitra, D. 2017, *JApA*, 38, 52  
 Qiao, G.J.; Lee, K.J.; Wang, H.G.; Xu, R.X.; Han, J.L. 2004a, *ApJL*, 606, L49  
 Qiao, G.J.; Lee, K.J.; Zhang, B.; Xu, R.X.; Wang, H.G. 2004b, *ApJL*, 616, L127  
 Radhakrishnan, V.; Cooke, D.J. 1969, *ApL*, 3, 225  
 Rankin, J.M. 1983, *ApJ*, 274, 359  
 Rankin, J.M. 1986, *ApJ*, 301, 901  
 Rankin, J.M. 1990, *ApJ*, 352, 247  
 Rankin, J.M. 1993, *ApJ*, 405, 285  
 Rankin, J.M. 1993b, *ApJS*, 85, 145  
 Rankin, J.M.; Ramachandran, R. 2003, *ApJ*, 590, 411  
 Rankin, J.M.; Wright, G.A.E.; Brown, A.M. 2013, *MNRAS*, 433, 445  
 Ruderman, M.A.; Sutherland, P.G. 1975, *ApJ*, 196, 51  
 Skrzypczak, A.; Basu, R.; Mitra, D.; Melikidze, G.I.; Maciesiak, K.; Koralewska, O.; Filothodoros, A. 2018, *ApJ*, 854, 162  
 Smith, E.; Rankin, J.M.; Mitra, D. 2013, *MNRAS*, 435, 1984  
 Smits, J.M.; Mitra, D.; Kuijpers, J. 2005, *A&A*, 440, 683  
 Srostellik, Z.; Rankin, J.M. 2005, *MNRAS*, 362, 1121  
 Swarup, G., Ananthakrishnan, S., Kapahi, V. K., *et al.* 1991, *Current Science*, 60, 95  
 Szary, A.; van Leeuwen, J. 2017, *ApJ*, 845, 95  
 Timokhin, A. 2010, *MNRAS*, 408, 41  
 Vivekanand, M.; Joshi, B. C. 1997, *ApJ*, 477, 431  
 van Leeuwen, A.G.J.; Kouwenhoven, M.L.A.; Ramachandran, R.; Rankin, J.M.; Stappers, B.W. 2002, *A&A*, 387, 169  
 Weltevrede, P. 2016, *A&A*, 590, 109  
 Wright, G.A.E.; Fowler, L.A. 1981, *MNRAS*, 101, 356  
 Wright, G.A.E.; Weltevrede, P. 2017, *MNRAS*, 464, 2597